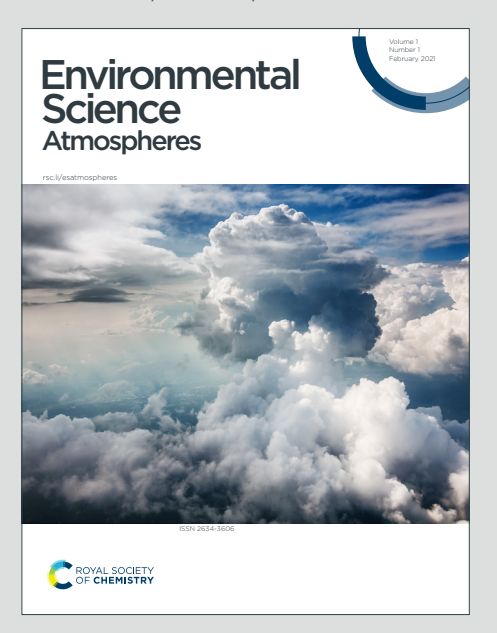


Environmental Science Atmospheres



Accepted Manuscript

This article can be cited before page numbers have been issued, to do this please use: L. S. P. Nguyen, N. D. Thanh, H. Q. Le, G. R. Sheu and H. T. To, *Environ. Sci.: Atmos.*, 2025, DOI: 10.1039/D5EA00094G.



This is an Accepted Manuscript, which has been through the Royal Society of Chemistry peer review process and has been accepted for publication.

Accepted Manuscripts are published online shortly after acceptance, before technical editing, formatting and proof reading. Using this free service, authors can make their results available to the community, in citable form, before we publish the edited article. We will replace this Accepted Manuscript with the edited and formatted Advance Article as soon as it is available.

You can find more information about Accepted Manuscripts in the <u>Information for Authors</u>.

Please note that technical editing may introduce minor changes to the text and/or graphics, which may alter content. The journal's standard <u>Terms & Conditions</u> and the <u>Ethical guidelines</u> still apply. In no event shall the Royal Society of Chemistry be held responsible for any errors or omissions in this Accepted Manuscript or any consequences arising from the use of any information it contains.



View Article Online DOI: 10.1039/D5EA00094G

PAPER

- Received 00th January 20xx. Accepted 00th January 20xx

- DOI: 10.1039/x0xx00000x

sites in a southeast asian megacity using generalized additive model Ly Sy Phu Nguyen,*ab Duc Thanh Nguyen,ab Le Quoc Hau,ab Guey-Rong Sheu, *c To Thi Hiena,b Particulate-bound mercury (PBM) plays a critical role in atmospheric mercury (Hg) cycling, yet its complex spatiotemporal variability and potential driving factors remain insufficiently understood, particularly in the Southeast Asia (SEA) region. This study reported year-round (May 2022 to April 2023) data of PBM at an urban (Nguyen Van Cu: 59.81 ± 29.15 pg m⁻³) and a suburban site (Can Gio: $26.4 \pm 9.59 \, pg \, m^{-3}$) in southern Vietnam. Distinct seasonal trends were observed at both sites, with elevated PBM concentrations in the dry season (November-February), likely driven by changes in source origin and transport 22 paths of air masses. Lower PBM concentrations in the wet season (July-September) may result from enhanced removal by wet deposition, whereas limited rainfall in the dry season reduces this effect, leading to higher 25 concentrations. We employed Generalized Additive Models (GAM), which 26 effectively captured nonlinear relationships between PBM and meteorological-27 chemical covariates. GAMs explained 87.7% of PBM variance in the urban area and 41.6% in the suburban area, indicating better model performance in urban vs suburban areas. In the urban area, metals (i.e. Cr, Sr, Pb, and V) were the dominant contributors (36.7%), suggesting influence from industrial and traffic-

related sources. In contrast, PBM at the suburban site was mainly modulated by temperature (60.8%), Zn (21.3%), and planetary boundary layer height (17.9%), pointing to the significance of atmospheric processes over local

Revealing the discrepancy in potential driving factors of particulate-bound

mercury between urban and suburban

^{a.} Faculty of Environment, University of Science, Ho Chi Minh City, Vietnam.

b. Vietnam National University, Ho Chi Minh City, Vietnam.

^{c.} National Central University, Taiwan.

^{*}Corresponding authors

Supplementary Information available: [details of any supplementary information available should be included here]. See DOI: 10.1039/x0xx00000x

emissions. Our findings highlight the utility of GAM in resolving complex **36**M- attribution and informing targeted mercury mitigation strategies. DOI: 10.1039/D5EA00094G environment interactions and indicate its potential for advancing source

Environmental significance

35

37

38

39

40

ੂੰ48 30

.<u>≅</u>50

13

14

56

57

58

59

60

61

62

63

Published on р 849

Particulate-bound mercury (PBM) is a highly toxic form of atmospheric mercury, capable of regional-scale transport through complex atmospheric processes, posing substantial risks to ecosystems and public health. However, its behavior in tropical urban-suburban settings remains poorly characterized. This study provides the first year-round observational dataset of PBM in southern Vietnam, revealing distinct seasonal patterns and site-specific drivers. By employing Generalized Additive Models, we indicated the effectiveness of data-driven approaches in disentangling complex PBM-environment relationships. Our findings suggest the contrasting roles of anthropogenic emissions and meteorological processes in shaping PBM levels in urban and suburban areas. These insights are essential for improving source attribution, supporting air quality management, and informing mercury mitigation strategies in rapidly developing regions of Southeast Asia.

1. Introduction

Mercury (Hg) is a persistent heavy metal with $high_{66}$ bioaccumulation potential, which has been shown to have 67 significant adverse effects on human health and ecosystems. 1-368 Although it comprises less than 5% of total atmospheric Hg,69 particulate-bound mercury (PBM) plays a pivotal role in 70 environmental processes owing to its relatively high deposition₇₁ velocity and its function as a crucial vector connecting the 72atmosphere with other environmental compartments. 1,4 PBM₇₃ originates from a mix of anthropogenic and natural sources and shows large differences in source contributions between different 75 regions (e.g., urban vs suburban).^{5,6} Key anthropogenic sources of PBM include combustion processes (e.g., coal combustion), metal production, and various industrial activities, while natural sources involve volcanic eruptions and natural biomass burning. 6-9 These emissions are further influenced by atmospheric processes such as oxidation, adsorption, and condensation. 10-12 81 East and Southeast Asia (SEA) contribute approximately $38.7\%_{82}$ global anthropogenic Hg emissions,

industrialization and urbanization.^{2,13} Studies indicated the critical role of the East and SEA region in the global Hg cycle. 6,13,14 While research in East Asia has advanced understanding of PBM source and transport, significant uncertainties remain, particularly regarding PBM variability in SEA region. 6,15-17 This shortage is mainly due to limited PBM data in SEA and the diverse emission sources. complex atmospheric chemistry, and region-specific meteorological conditions.¹⁸ Improved characterization of PBM behavior in SEA is essential for identifying dominant sources and informing effective regional mitigation policies.

Source apportionment of PBM has traditionally relied on multivariate techniques such as Principal Component Analysis (PCA) and Positive Matrix Factorization (PMF). 18-21 While PCA reduces data dimensionality, it assumes linearity and permits negative loadings, limiting its interpretability.²² PMF addresses nonnegativity but still assumes linearity, requires pre-specifying the number of sources, and is sensitive to outliers. 20,23,24 To address the nonlinear relationships inherent in environmental Generalized Additive Models (GAM) have been increasingly applied in air pollution research, including atmospheric Hg.²⁵⁻²⁸ GAMs offer

85

86

87

88

89

90

bution 3.0 Unported 98 20 Unported

95

g 96

ರ _ഉ97

aCrea 86

99 1999

1 200<u>₹</u>

∄02

14

106

107

108

109

110

111

112

113

114

Downloaded

2025.

Published on 30

Open Access Article.

ARTICLE

Journal Name

relationships between pollutant concentrations an2d16 environmental/meteorological variables without requiring prio1i17 assumptions about the functional form of these relationships. 25, 4618 For atmospheric Hg, Wu et al.27 applied GAM to quantify the 19 contribution factors on TGM concentrations in Beijing, attributing 20 47.1% of the observed TGM variability to meteorological drivers. **\(\Delta 21 \)** a subsequent study, Wu et al.²⁸ employed GAM to illustrate th 22 Hg mitigation strategies in rapidly growing urban centers across the effects of COVID-19 lockdown measures from meteorologic **al23** influences such as relative humidity and temperature on TGM. These studies indicated the flexibility of GAM in environmental

modeling for capturing nonlinear environmental responses However, the use of GAM for PBM remains limited in the SEA region as well as in the literature. This represents a critical gap in the $\begin{array}{c} 127\\ \text{current understanding of PBM dynamics and their interactions with} \end{array}$ 128 environmental factors. 129

In this study, we present a year-round observational dataset 130(May 2022 - April 2023) on PBM concentrations and the elements 131of total suspended particles (TSP) obtained from two selected 132monitoring sites (urban and suburban) in Ho Chi Minh City (HCMC) $_{133}^{\circ}$ Vietnam. From the perspective of particle size, TSP refers to the 34 total fraction of airborne particles collected by a sampler without a size-selective inlet, typically capturing particles with aerodynamic 136diameters up to ~100 μ m.²⁹ Unlike PM_{2.5} or PM₁₀, TSP therefore 237 encompasses both coarse and fine particles without a specific cutoff 138limit. HCMC is a representative megacity of Southeast Asiq,39 characterized by rapid urbanization, high population density, and 140complex emission profiles. For the first time in this region, these 41data are integrated into a GAM model to explore key atmospherica? processes influencing PBM. The primary aims of our study are: $\binom{1}{143}$ Tο characterize the spatiotemporal variations

a flexible statistical framework that can model complex, nonlinear15 concentrations across contrasting environments; (2) To investigate DOI: 10.1039/D5EA00094G the relationships between PBM, chemical constituents of TSP, and meteorological parameters; and (3) To apportion and quantify the relative contributions of various anthropogenic and natural emission sources to PBM levels at both sites. The results from this study will not only enhance the understanding of PBM dynamics in SEA but also offer valuable insights for the development of targeted

2. Materials and methods

2.1. Site description and TSP sampling

In this study, TSP samples were collected from two sites in HCMC (Fig. S1), representing contrasting environmental contexts: an urban site (Nguyen Van Cu - NVC; 10.762°N, 106.680°E) and a suburban/coastal site (Can Gio - CG; 10.402°N, 106.947°E). At NVC site, TSP sampling was conducted on the rooftop of an 11-story building at the University of Science, VNU-HCM. The site is situated approximately 10 meters from a major multi-lane roadway and is influenced by anthropogenic emissions, particularly from vehicular traffic.30 In contrast, the CG site is positioned on the second floor of Can Thanh High School in Can Gio District, approximately 50 km southeast of central HCMC. This site located in a low-density residential area, about 40 meters from a local road and 400 meters inland from the coastline and is surrounded by extensive mangrove forests (Fig. S1). It is relatively isolated from major anthropogenic emission sources.31,32 These monitoring sites have been applied in numerous atmospheric studies^{18,32,33} and are considered representative of urban and suburban/coastal atmospheric environments in HCMC.

At two monitoring sites, a total of 8 TSP samples were collected at atomic absorption spectrometry (AAS). Monthly blank values were each month, with sampling dates properly scheduled between th 275 10th and 20th of each month, from May 2022 to April 2023. At the 76 CG site, TSP was collected using a high-volume air sampler (Mod&177) 120H, Kimoto Electric Co., Japan) operating at 600 L min⁻¹ with gla\$78 fiber filters (GFF; Advantec GA-55, 203 × 254 mm). At NVC, a high-79 volume sampler (Model HV-500R, Sibata Scientific Technology Ltd. 80 Japan) operated at 500 L min⁻¹ using GFFs (Advantec; 110 mth81 diameter. The flow rate accuracy of both sampling instruments wals 2 lower than ±5% of the set value, as specified by the manufacturers. 183 All filters were pre-combusted at 400°C for 8 hours to eliminate 184 residual Hg. Filters were conditioned at 25 ± 2°C and 40 ± 5% RH for 185 48 hours before and after sampling. Samples were stored at -20°C 186 until analysis. Field blanks were prepared, stored, and analyzed 187 following the same protocol to assess potential contamination 188 during sampling and handling. All procedures followed strict QA/QC 189 protocols, including the use of field and laboratory blanks 190 throughout the campaign. Detailed protocols for filter preparation 191 and sample handling are described in previous studies. 18,23,33 192

2.2. Mercury and elements analysis

144

145

146

147

148

149

150

₹51

252

₹53

. ₹54

≨55

1256

¥57

₫58

£61

‡62

64

166

167

168

169

170

171

172

173

on 08/11/25 02:28:01

Downloaded

30 **⊉**59

on

Published **1**60

Open Access Article.

194 The concentrations of Hg in GFF samples collected in this study 195 were analyzed at the laboratory of Dr. Guey-Rong Sheu, National 196 Central University, Taiwan. Total Hg was quantified using a MA-3 197 Solo thermal decomposition analyzer (Nippon Instruments 198 Corporation, Japan) in accordance with USEPA Method 7473, a 199 widely adopted protocol for Hg determination. 18,34,35 The thermal 200 protocol involved an initial heating at 350°C to remove moisture and volatile organics, followed by a ramp to 850°C to decompos201 and release Hg. Gaseous Hg was transported to a go 2002 amalgamation trap, thermally desorbed at 600°C, and quantified b203

DOI: 10.1039/D5EA00094G subtracted to obtain PBM concentrations. Method blanks were < MDL (0.05 ng), with liquid standard recoveries of $99 \pm 3\%$ (n = 31). Certified reference materials (NIST SRMs 1648a and 2685c) showed recoveries of $99.8 \pm 7.2\%$ and $95.7 \pm 3.0\%$, respectively. These results confirm the method's high precision and analytical reliability. The operational principles and standard QA/QC procedures of the analytical method have been thoroughly documented in previous literature.18

Elemental analysis was conducted via wet acid digestion followed by inductively coupled plasma mass spectrometry (ICP-MS). 20 elements (Al, As, Ba, Ca, Cd, Co, Cr, Cu, Fe, K, Mg, Mn, Ni, Pb, Sb, Se, Sr, Ti, V, Zn) were quantified according to U.S. EPA Methods 6020B and 200.8 (Rev. 5.4). Samples were digested using a 2:1 (v/v) mixture of HNO₃ and HCl in Teflon vessels, employing microwave-assisted digestion. 23,36 The digested solutions were filtered through 0.45 µm PTFE membranes and analyzed using an Agilent 7700x ICP-MS system (Agilent Technologies, USA). Analytical accuracy was validated with the certified reference material SRM 1684a, achieving recovery rates between 80% and 120% for all 20 elements. Reagent blanks were included to control contamination, and blank values were subtracted to obtain corrected concentrations. Further instrumentation and analytical details are available in our previous study.²³ In this study, elemental data were mainly applied to incorporate into the GAM framework as predictor variables to identify potential drivers of PBM variability rather than to explore the contribution to TSP sources.

In addition, meteorological variables, including temperature (T) and relative humidity (RH), were recorded at sampling sites. Planetary boundary layer (PBL) height and surface-level PM_{2.5}

205

206

207

208

209

210

Ž11

212

213

₹14

≩15

216

₹17

219 Published

220

12

!3

225

226

227

228

229

230

231

232

steps:

Downloaded on 08/7

30 **2**18

Open Access Article.

244

245

ARTICLE

View Article Online DOI: 10.1039/D5EA00094G

Journal Name

Retrospective analysis for Research and Applications, Version 2) reanalysis, which assimilates satellite observations from infrared, 235 microwave, and GPS radio occultation sources. 37,38 A full system 236 description is available in Buchard et al.³⁹ In addition, this study 237 employs the HYSPLIT (Hybrid Single-Particle Lagrangian Integrated 238 Trajectory) model to analyze the backward trajectories of air masses 239 to two study areas. Five-day backward trajectory simulations were 240 conducted for each month within the study period, aiming to 241 identify the origins and movement patterns of the air masses to 242 these locations. 40,41 243

2.3. Building the GAM model

In this study, GAM was used to investigate the relationships 246 between PBM concentrations and chemical elements, as well as 247 meteorological variables. GAM offers a straightforward and interpretable model for representing the associations between 248 dependent variable and independent variables.⁴² Specifically, the 249 model is expressed as follows: 250

$$g(\mu_i) = X_i \theta + f_1(x_{1i}) + f_2(x_{2i}) + \dots + f_n(x_{ni}) + \xi_i$$
 (1) 251

252 where i denote the ith observation, g is the link function, and 253 μ_i represents the expected value of the dependent variable, 254 defining the relationship between the linear predictor on the right-255 hand side of Equation (1) and the dependent μ_i . The term $X\theta$ 256 corresponds to the parametric component of the model, capturing 257 the relationship with independent variables characterized by linear 258 relationships. The function f(x)denotes the smooth term 259 associated with nonlinear predictors. 260 The model construction procedure was carried out in the following 61

concentrations data were derived from the MERRA-2 (Modern-Et233 Step 1: Data preparation

The dataset used in this study was split into two subsets corresponding to the two monitoring locations. Each sample record includes concentrations of PBM and 20 elements (Al, As, Ba, Ca, Cd, Co, Cr, Cu, Fe, K, Mg, Mn, Ni, Pb, Sb, Se, Sr, Ti, V, and Zn) in TSP alongside three meteorological variables: T (°C), RH (%), and PBL (m). Precipitation was not included as a predictor in the GAM model due to the lack of high-resolution data for the entire study period and its strongly discontinuous distribution, which reduces model stability. Similarly, other meteorological parameters (i.e., wind speed, wind direction, and atmospheric pressure) were excluded due to data discontinuity and incomplete coverage across the study period. All elemental and meteorological datasets were subjected to standardized quality control procedures. Outliers beyond ±2.5 standard deviations were capped at the respective thresholds.

Step 2: Variable selection

To evaluate the normality of the input data, the Shapiro-Wilk test was employed to assess the conformity of each variable to a Gaussian distribution. Details of the test outcomes and the corresponding transformations applied to approximate normality prior to inclusion in the GAM model are provided in Table S1. Penalized cubic regression splines were utilized to smooth the continuous predictors, offering a flexible yet controlled means of capturing nonlinear relationships while minimizing the risk of overfitting.^{26,43} Model optimization was guided by generalized cross-validation (GCV), which balances model complexity with predictive performance.²⁸ Predictor significance was evaluated using p-values, serving as diagnostic metrics for model refinement. The initial full model included all candidate variables, followed by

iterative removal of non-significant terms based on their statistic 291 respectively. In contrast, PBM concentrations displayed marked DOI: 10.1039/D5EA00094G relevance.26-28 292 spatial variation. The mean PBM concentration at NVC was 59.81 ± 29.15 pg m⁻³, more than twice the level observed at CG, which Step 3: Model Evaluation 294 averaged 26.4 ± 9.59 pg m⁻³. This disparity highlights the stronger To rigorously evaluate the predictive performance an295 influence of urban emissions (i.e. anthropogenic emissions) on PBM generalizability of the GAM constructed for the NVC and C296 levels within the city center. datasets, a 10-fold cross-validation procedure was implemented. Table 1 compares the PBM level in HCMC to other sites This approach is widely recognized in statistical learning⁴⁴ 298 worldwide. In general, PBM concentrations in HCMC were particularly in GAM applications^{43,45}, and is increasingly employed 299 considerably lower than those reported in several heavily in environmental and ecological modeling.⁴⁶⁻⁴⁸ Each dataset was industrialized cities. 19,49,50 For instance, Beijing, China reported 300 randomly divided into 10 equal subsets. In each iteration, 9 subsets mean levels of 210.1 ± 146.2 pg m⁻³, approximately 3.5 times higher 301 were used to train the model, while the remaining subset was used 302 than in HCMC.50 Similarly, Kathmandu, Nepal recorded for validation. This process was repeated 10 times, ensuring that concentrations of $850.5 \pm 926.8 \text{ pg m}^{-3}$, exceeding HCMC levels by a 303 each subset served as the validation set once. Model performance 304 factor of 14 (Guo et al., 2021). Urban centers in developed regions in each fold was quantified using the coefficient of determination 305 such as Detroit, USA (20.8 ± 30 pg m⁻³) and Seoul, South Korea (23.9 (R2), and the mean R2 across all folds was reported as a robust 306 ± 19.6 pg m⁻³) also reported higher/comparable values, indicator of the predictive capability of the model.⁴⁶ In addition to 307 respectively.51,52 Comparable trends were observed in Shanghai, assessing the adequacy of model assumptions and supporting the 308 China (560 \pm 220 and 330 \pm 90 pg m⁻³;49), and Xi'an, China (640 \pm validity of inference, diagnostic checks were conducted, including 309 540 pg m⁻³;53). These elevated PBM concentrations have been quantile-quantile (Q-Q) plots to evaluate the normality of residuals 310 attributed to emissions from coal combustion, metallurgical and autocorrelation function (ACF) plots to examine residual activities, and other fossil fuel-related sources. 49,53 Despite its status 311 independence (Wood, 2017). as a major economic hub, HCMC (particularly NVC) appears to 3. Results and discussion experience relatively limited direct impact from such heavy industrial activities compared to other megacities. 3.1. Characterization of PBM data 315 Suburban comparisons also reveal important contrasts. For Between May 2022 and April 2023, a total of 192 TSP samples 316 example, Xiamen, China reported PBM were collected from two monitoring sites in HCMC: 97 samples from 317

Between May 2022 and April 2023, a total of 192 TSP samples 316 were collected from two monitoring sites in HCMC: 97 samples from 317 NVC (urban) and 95 samples from CG (suburban). Meteorological 318 conditions were generally similar between the two suburban sites 319 (t-test, p>0.05), with mean T of 29.0 \pm 1.2°C at NVC and 30.9 \pm 1.7°C 320 at CG, and average RH values of 73.6 \pm 6.8% and 69.4 \pm 5.3%,

example, Xiamen, China reported PBM concentrations approximately 6.7 times higher than those at CG.⁵⁴ Dhulikhel, Nepal recorded levels of $108.7 \pm 86.2 \text{ pg m}^{-3}$, about four times those measured at CG.¹⁹ Similarly, PBM levels reported at Zabrze, Poland (65.5 \pm 53.7 pg m⁻³) also exceeded the concentrations at CG,

262

263

264

265

266

267

₹68

269

270

₹71

274

₹75

ଛ ⊉76

285

286

287

288

289

290

Published

322

323

324

325

326

327

₹28

₹29

₹30

₹31

\$32

₹33

3 3€34

₹35

₹37

≸38

∄39

1

343

344

345

346

347

348

349

350

351

PBM levels.

on 08/11/25 02:28:01

Downloaded

30 ₹36

on

Open Access Article. Published

364

365

366

367

368

369

ARTICLE

Journal Name

highlighting regional variation in emission sources and atmospher 252 related sources. 60-62 Conversely, in the suburban area, although Ca processes. 55,56 In contrast, the concentration observed at CG (263453) ± 9.59 pg m⁻³) is comparable or higher than those in cleaner or les 54 industrialized coastal settings such as Nova Scotia, Canada (2.32355) 3.09 pg m⁻³), Beltsville, USA (8.6 \pm 56.8 pg m⁻³), high mountain **3.56** central Taiwan (3.1 \pm 8.5 pg m⁻³), Taoyuan City, Taiwan (18.7 \pm 863857 pg m⁻³), and Okinawa, Japan $(2.6 \pm 3.6 \text{ pg m}^{-3})$ (Table 1).^{3,5,17,56} The $\frac{3}{2}$ 58 comparisons indicate the relatively moderate level of PBM at C3.59 suggesting limited influence from heavy industrial activities an360 reflecting a suburban emission profile distinct from urba\(\frac{3}{6} 61 \) atmospheric transport.\(\frac{8}{,23},64 \) industrialized regions. It is worth noting that the comparisons of 362 PBM concentrations (Table 1) were derived from measurements 363

based on different particle size fractions (i.e., TSP, PM₁₀, and PM_{2.5}).

Consequently, certain variability is inevitable due to the size-

dependent partitioning behavior of mercury.⁵⁸ Moreover, distinct

physical and chemical characteristics associated with each particle

size fraction may further contribute to the observed variations in

Fig. 1 illustrates the relative distribution of element 3170 composition in TSP collected from urban and suburba 371 environments. In urban site, Ca was the most dominant elemen 3,72 accounting for 41.12%, followed by Fe (21.98%), Al (13.26%), 373 (10.07%), and Mg (7.96%) (Fig. 1a). This compositional profi №74 indicates a predominant influence from crustal and anthropogen £75 contributions, particularly construction, vehicular emissions, and 76 industries using heavy metals.^{23,32,36} In contrast, in the suburban resuspended road dust, characteristic of densely populated urba\377 areas. 18,30,36 The elevated levels of Fe and Al indicate mineral dus 78 inputs, while K and Mg may reflect inputs from biomass burning an 379 soil-derived particles.^{8,23,59} Additionally, trace elements such as **Z380** (2.97%) and Cu (10.51%), found within the category of oth $\frac{2}{3}$ 81 Ti (r = 0.53), and Al-Ca (r = 0.52), further confirm the predominance elements also suggest the influence of industrial activities or traffi882 of soil-derived sources. Meanwhile, the significant correlations

DOI: 10.1039/D5EA00094G remained the dominant element (45%), Mg emerged as the second most abundant at 24.87%, surpassing Fe (6.68%) (Fig. 1c). This shift suggests a different source profile, potentially related to greater vegetation cover, proximity to the coast, lower human activity intensity, and reduced construction emissions. 32,36,63 AI (9.69%) and K (7.86%) also contributed significantly, along with Cu (3.72%) and Zn (1.3%), which may originate from local anthropogenic activities such as agricultural practices, domestic combustion, or long-range

The distribution of trace elements in TSP at the urban and suburban areas shows distinct differences in the distribution and relative abundance of elements between urban and suburban areas. In the urban area, elements such as Pb (18.09%), Mn (15.66%), and Cu (10.51%) dominate (Fig. 1b), reflecting the influence of anthropogenic activities, particularly emissions from traffic, industrial activities, and construction. 65-67 The correlation analysis among the measured elements was conducted to explore potential associations and shared origins (Tables S2 and S3). Meanwhile, strong correlations among transition metals (i.e., Cr, Mn, and Co) further confirm their common anthropogenic origin (r = 0.82-0.91; p < 0.05). Likewise, the significant associations between Pb-Cd (r = 0.84), As-Se (r = 0.79), As-Cd (r = 0.79), and Cd-Sb (r = 0.79) 0.77) suggest concurrent emissions from combustion sources and area, elements such as Ti (23.18%) and Mn (18.75%) are more prominent (Fig. 1d), indicating a greater influence from natural sources such as soil dust and vegetation.^{23,32} The moderate correlations among crustal elements, for instance, Al-K (r = 0.55), Al-

427

Mn (r = 0.51) likely indicate the influence of anthropogen 4.14activities, possibly traffic-related emissions (Table S3). Additionall 4,15 Pb (13.02%) is present at lower levels, indicating less contributio 416 from industrial emissions compared to the urban area. ^{23,32,36} The ⁴¹⁷ differences illustrate spatial variability in elemental compositio 418 between the two environments, suggesting differences 419 population density and surrounding land use characteristics. 32,63,68 420 These observations are crucial for understanding the behavior of 421 PBM, as the chemical environment in which PBM exists can 422 influence its transformation, transport, and potential health 423 impacts. 11,18,69 Therefore, characterizing elemental distribution 424 patterns is a key foundation for interpreting PBM dynamics in 425 complex urban-suburban transitions. 426

383

384

385

386

387

388

389

₹90

₹91

<u>ਤੋ</u>ਂ92

₹93

₹94

₹95

₹96

₹98

399

400

2)3

405

406

407

408

409

410

411

412

Downloaded

30

Published

3.2. Seasonal variation and potential driving factors

428 Fig. 2 reveals a pronounced seasonal pattern of PBM 429 concentrations at both urban and suburban sites in HCMC. During 430 the major rainy season (July-September), mean PBM concentrations 431 were lower, averaging 38.5 ± 12.4 pg m⁻³ at NVC and 19.8 ± 10.7 pg 432 m⁻³ at CG. In contrast, the major dry season (November-February) exhibited elevated levels at the urban site (109.0 ± 50.9 pg m⁻³), and suburban (40.6 ± 22.2 pg m⁻³). The seasonal variation in PBM34 concentrations observed in both urban and suburban sites in HCM235 reflects the combined influence of rainfall-driven removal an436 seasonal air mass transport dynamics. 18,23,32 During the rain 437 season, frequent and intense rainfall events associated with the 38 Southwest monsoon promote efficient wet scavenging of PBM,39 resulting in generally lower concentrations. Rainfall facilitates th 440 removal of PBM, especially in tropical environments where41 convective systems are prevalent.^{4,14,18} In contrast, during the d4/42 atmospheric transport was not the primary contributor to the

among Fe-Mn (r = 0.69), Ti-Mn (r = 0.74), Zn-Fe (r = 0.60), and ZA13 season, limited rainfall reduces atmospheric cleansing, allowing DOI: 10.1039/D5EA00094G PBM to accumulate in the boundary layer, resulting in an elevation of PBM levels. In addition, meteorological parameters such as T and RH remained relatively constant across seasons (p > 0.1, ANOVA), suggesting that local meteorological variability had limited direct influence on PBM seasonal dynamics.

> Furthermore, seasonal variations in prevailing air mass transport patterns, governed by the East Asian monsoon system, play a critical role in shaping atmospheric composition in HCMC. 32,33,70 Results from backward trajectory analyses (Fig. S2, S3) indicate that during the dry season, air masses predominantly originate from the northeast, possibly originating from highly industrialized regions across continental East Asia. 14,71,72 These air masses could carry high PBM levels, enhancing background PBM levels across both urban and suburban sites in HCMC.5,17,70 In contrast, during the rainy season, the sampling sites are primarily influenced by southwesterly air masses originating over the ocean (Fig. S2, S3), which transport relatively clean maritime air to HCMC. Similar seasonal atmospheric Hg trends linked to continental outflow have been reported across East Asia, including Taiwan, Japan, South Korea, and Vietnam. 5,17,70,73

> Notably, during the rainy season, a pronounced difference in PBM concentrations was observed between the urban and suburban sites in June, with the NVC site recording a seasonal maximum of 76.5 ± 29.5 pg m⁻³, approximately 64% higher than its rainy season mean value (Fig. 2). In contrast, no corresponding peak was detected at the CG site (Fig. 2). Analysis of backward trajectories and surface PM_{2.5} revealed comparable air mass origins for both sites during this period, suggesting that long-range

444

445

446

447

448

449

₹50

451

₹52

₹53

₽54

455

456

.siu **46**1

12

43

465

466

467

472

on 08/11/25 02:28:0

Downloaded

2025. 2025. 2025.

€ 458

on

Published is lice

Journal Name

ARTICLE

elevated PBM levels at NVC (Fig. S2, S3). Results from surface PM 473 most of the variability in PBM concentrations at this site. In contrast.

DOI: 10.1039/D5EA00094G the much lower adjusted R² at CG implies a weaker model fit,

absence of a similar increase at the suburban site supports the 75 potentially due to unaccounted site-specific factors or greater

interpretation that local accumulation processes, likely driven b476

stagnant meteorological conditions, predominated at the urba477

site. $^{32,33}\,\text{This}$ interpretation is further supported by meteorologic $478\,$

data, which show that June experienced the lowest mean wind 479 speed of the season (1.1 m s⁻¹), considerably lower than values

480 recorded in other months (1.5-1.7 m s⁻¹), favoring the buildup of air

481 pollutants. In summary, the seasonal variability of PBM in HCMC is

482 governed by a complex interplay of local accumulation processes,

483 monsoonal shifts in prevailing air mass origin, and regional-scale

484

pollutant transport. While local emissions dominate during 485

stagnant conditions in the wet season, transboundary transport \$486>

becomes increasingly significant during the dry season, highlighting $487 \,$

the importance of considering both local and regional scales in 488

atmospheric Hg management strategies.

3.3. Analysis and evaluation of GAM performance 490

491

Based on the variable selection results presented in Table S4, a 492

total of 19 independent variables (PBL height and 18 elements) 493

were retained for the NVC dataset, while only 3 variables (PBL, T, 494

and Zn) were retained for CG (p < 0.05, summary function). Model 495

performance metrics are summarized in Table S5. The GAM 496

indicated strong correlations between the selected predictors and

PBM concentrations, with R² reaching 90.8% for NVC and 94.5% for

468 CG, indicating robust initial fits. 28,43,74 However, the explanato 498

469 power of the models, as measured by adjusted R^2 , differe 499

470 markedly: 0.73 at NVC and only 0.32 at CG (Table S5). The adjuste 500

471 R² of 0.73 at NVC indicates a strong and reliable mod 501

performance, suggesting that the selected predictors capture 602

the much lower adjusted R² at CG implies a weaker model fit, potentially due to unaccounted site-specific factors or greater variability in local conditions. This contrast suggests a reduced

ability to generalize the influencing factors of PBM concentrations

in suburban environments.^{75,76}

The higher explanatory capacity of the NVC model can be attributed to the broader spectrum of input variables, which likely captured key emission sources and meteorological influences. In contrast, the limited predictor set for CG constrained the model's ability to represent PBM variability. Comparative assessment with prior studies further highlights the improved performance of the current urban model. The statistical model explained 87.7% of the variance in PBM concentrations, with the adjusted R² reaching 0.73 at the NVC site, indicating superior performance compared to the model of TGM in the Beijing-Tianjin-Hebei region, which achieved an adjusted R² = 0.62 and explained 63.2% of the variability.²⁸ In contrast, at the CG site, the statistical model showed a considerably lower predictive capacity, explaining 41.6% of the variance in PBM concentrations, with the adjusted R² reaching 0.32, consistent with the findings of Wu et al.²⁷, where the model explained 56.7% of the TGM variability (adjusted $R^2 = 0.551$). It should be noted that our model was developed for PBM, while the referenced studies modeled TGM, which may inherently differ in their atmospheric behavior, influencing model sensitivity and explanatory capacity.

These results emphasize the critical importance of incorporating a diverse array of explanatory variables. The limited inclusion of local environmental indicators (e.g., land use, vegetation cover, potential emission sources) may have further hindered model performance at CG.^{25,68,77} Diagnostic analyses from

Journal Name

544

545

ARTICLE

Fig. S5 and S6 indicate that both GAM models at the NVC and C533 sites satisfy key statistical assumptions and are well-suited to the 34 environmental characteristics of each location. At NVC, the 35 residuals follow a normal distribution, are homogeneous 5/36 dispersed around zero, and the predicted values align closely wi \$37 observations, demonstrating high model accuracy and strong 38 predictive capacity. At CG, the residuals also exhibit a norm 539 distribution, with a symmetric histogram and Q-Q plot, and no 40 systematic bias across fitted values. Overall, both models as 41 statistically reliable and highlight the flexibility of GAM in analyzing 42 PBM across contrasting environmental settings. 43,78,79

3.4. Relationship analysis results

503

504

505

506

507

508

509

§10

§11

<u>ਤੋਂ</u>12

<u>Ş</u>13

§14

515

516

§18 Published

₹19

<u>=</u>3

525

526

527

528

529

530

531

532

Downloaded on 08/7

30 §17

Fig. 3 and S8 show the nonlinear relationships between PBIG46 and other parameters (i.e. elements and meteorology) at the NV\$47 site, revealing complex interactions between emission sources ans 48 atmospheric processes. Several crustal (e.g., Al, Ti; Fig. S8) angl49 anthropogenic elements (e.g., Cd, Co, Cr, Cu, Pb, Sb) exhibite (50) statistically significant positive associations with PBM level5,51 suggesting their potential role in PBM-enriched source sectors such 52 as traffic-related emissions, coal combustion, and industrial53 activities at the sampling site. 18,23,32 This finding aligns with previous 54 GAM-based studies, where key emission sectors (e.g., cemen 555 power plants) exhibited significant relationships with Hg level 556 emphasizing the dominance of anthropogenic drivers 0957 atmospheric Hg variation. 27,28 By contrast, the PBL showed ans 58 inverse relationship with PBM (Fig. 3), consistent with enhance [59] vertical mixing and dilution under higher PBL conditions. 30,54 Similar 60 findings were reported by Wu et al.²⁸ in Beijing, China, indicating 61 that elevated PBL contributed to reductions in atmospheric Hg62 concentrations due to improved atmospheric dispersion.

DOI: 10.1039/D5EA00094G threshold-dependent nonlinearities. For instance, As and Ba displayed negative relationships with PBM at lower concentrations (<0.4 ng m⁻³ and <9 ng m⁻³, respectively; Fig. S8) but transitioned to positive relationships above these thresholds, indicating potential shifts in dominant sources or physicochemical partitioning behavior at higher loadings. These turning points may reflect saturation kinetics or source mixing, where low concentrations are dominated by background or natural sources, whereas elevated levels originate from combustion-related emissions. 10,12,80,81 Moreover, elements such as K, Sr, V, and Zn exhibited highly nonlinear trends with multiple inflection points (Fig. S8), suggesting their involvement in complex multiphase reactions or simultaneous contributions from diverse sources (e.g., biomass burning, traffic, and re-suspension processes). For instance, the GAM-based spline revealed that Zn exhibited a positive association with PBM concentrations at lower levels (up to ~125 ng m⁻³), after which the relationship plateaued or slightly declined (Fig. 3). This trend may reflect atmospheric saturation effects, particle-phase condensation limitations, or increased partitioning into coarse-mode particles at higher Zn concentrations, which may be less efficient at binding PBM.16 Additionally, in humid atmospheric conditions, Zn may facilitate heterogeneous reactions on particle surfaces or act as a catalyst in redox transformations of oxidized Hg.82,83 These findings imply the dual role of Zn as both a source tracer and a potential participant in secondary atmospheric processes influencing PBM formation and stability. Given the ubiquitous presence of traffic emissions in urban environments, the role of Zn as a proxy for this source category highlights the importance of traffic-related activities as a critical and persistent contributor to atmospheric Hg cycling.

Some elements (i.e., As, Ba, Fe, Mn, Ni, and Se), showed

564

565

566

567

568

569

ഉ 5970

₹71

<u>5</u>72

<u>5</u>73

574

5 75

⊊ 5√76

577

₹78 30

580

ß2

3

585

586

587

588

589

590

591

592

593

on 08/11/25 02:28:01

Downloaded

Published on § 79

Open Access Article.

Journal Name

showed similarly complex effects on PBM (Fig. 4). T showed 595 potential driving factors on PBM variabilities nonlinear association with PBM (Fig. 4a), characterized by a 596 negative response between 26-30 °C and a slight increase above 30 597 °C. The PBM-T relationship is inherently complex, as T controls the 598 gas-particle partitioning of Hg(II), lower temperatures favor 599 particle-bound fractions, whereas higher temperatures enhance 600 gaseous forms.^{9,12} Moreover, temperature variations may reflect 601 shifts in air mass origins (e.g., land-sea breeze), further influencing PBM levels. 12,84,85 The inverse relationship between PBL and PBM became evident above 330 m, reinforcing the role of boundary laye 03 dynamics in pollutant dilution. Notably, Zn at CG revealed 604 concentration-dependent relationship with PBM, positive 605 correlated below 125 ng m $^{\text{-}3}$ but negatively correlated beyond th 606threshold. This may indicate distinct PM binding capacities 607interactions under varying atmospheric chemical regimes. Simil 608 concentration-reversal effects of RH on TGM were reported by We⁰⁹ et al. 28 , where RH >80% enhanced aqueous phase reduction 10 processes and TGM re-emission, further illustrating the nonline $\11 behavior of Hg species in atmospheric systems.

In general, these results indicate the multifactorial nature δf^{13} PBM variability, governed by a combination of potential emission 14 source profiles and meteorological controls at both urban an $\[ext{0.15} \]$ suburban sites in HCMC. However, it should be acknowledged th \Re^{16} several nonlinear relationships revealed in the GAM remain partial §17 unexplained, particularly those involving threshold-dependent 18 behaviors and inflection points. These complexities may stem from 19unmeasured variables, insufficient temporal resolution, $\delta 20$ limitations in chemical speciation data. Consequently, our ability 621fully interpret the integrated influence of chemical an 622623 meteorological predictors on PBM remains constrained.

At the CG site, meteorological variables, including T and PB94 3.5. Contribution rates of independent variables, implications for DOI: 10.1039/D5EA00094G

ARTICLE

Table S6 shows the proportional contributions of factors influencing PBM concentration variability at NVC and CG sites, as determined by the VarImp function in the GAM model. 25,27,28 The relative importance of independent variables reveals striking contrasts between the two monitoring environments, highlighting the distinct roles of emission sources and meteorological controls in shaping PBM dynamics.

At the CG suburban site, meteorological conditions overwhelmingly dominated PBM variability, collectively accounting for 78.7% of the total variance (Fig. 5). Among these, T alone explained 60.8%, consistent with a strong positive, though nonlinear, association observed in the GAM spline. In addition, the PBL contributed 17.9% to PBM variation, reflecting the dispersive capacity of elevated mixing layers to dilute PBM concentrations, as noted in previous studies.32,33 These results indicate that in areas with limited direct emissions, PBM levels are primarily modulated by atmospheric dynamics.

In contrast, meteorological factors played a minor role at the urban NVC site, explaining only 1.2% of the variance (Fig. 5). This suggests that urban PBM levels are largely dominated by localized anthropogenic emissions. Indeed, anthropogenic sources contributed over 87.7% of the PBM variability at NVC, reflecting the complex contribution of combustion, industrial, and traffic-related emissions in a densely populated setting. Among combustionrelated sources, several elements showed high contributions to PBM at NVC, including Pb (8.8%), V (8.3%), Cd (5.5%), and As (5.6%), all commonly associated with fossil fuel burning.86,87 Pb and V are particularly indicative of the use of heavy oils and fossil fuels in both

and Sb (3.6%) also played significant roles within the combustio 655 developing targeted control strategies. related source group, although they are often considered to originate from mixed sources. K is a well-known tracer of biomass 657 burning, commonly found in plant ash and produced from the 658 combustion of wood, crop residues, or other organic materials.88,89 659 The prominent presence of K suggests the possible influence of local 660 open burning or resuspension of ash-derived dust within the urban 661 environment. In contrast, Se is typically found in emissions from 662 heavy oil and coal combustion, particularly from power plants and 663 industrial facilities using fossil fuels.90-92 664

624

625

626

627

628

629

630

€31

₹32

₹33

₫34

€35

€37

638

₫39

₫40

₫41

4

646

647

648

649

650

651

652

653

on 08/11/25 02:28:01

Downloaded **€**36

2025.

30

Published on

Open Access Article.

These elements also exhibited strong and significant positive 65 associations in GAM splines, suggesting their diagnostic importance in PBM variation. In addition, industrial-related elements, including 667 Sr (8.9%); Ni (5.8%), Co (3.9%), and Ba (0.6%), were also important 668 predictors at NVC. These originate from diverse industrial activities 669 such as steel production, alloy and battery manufacturing, pigment 670 and flame-retardant use. 36,61,93,94 Although anthropogenic 671 influences were predominant, natural sources contributed a non-672 negligible 11.1% to the PBM variation at the NVC site. Specifically, 673 elements such as Ti (5.4%), Fe (4.2%), and Al (1.5%), commonly 674 associated with crustal material, re-suspended soil dust, or biogenic 675 emissions, were linked to natural origins.^{36,63} These elements likely reflect background processes such as wind-driven resuspension, long-range transport of mineral aerosols, and interactions with natural surfaces. While their contributions were $\ensuremath{^{677}}$ $679\,$ provide a stable background signal and may influence PBM behavior 680 through surface reactivity or chemical partitioning mechanisms $\begin{array}{c} \textbf{681} \\ \textbf{Therefore, the combined effect of both anthropogenic and natural} \end{array}$

transportation and industrial processes. 36,59,65 K (4.6%), Se (4.6%), 54 inputs should be considered in assessing PBM dynamics and DOI: 10.1039/D5EA00094G

> Furthermore, non-combustion traffic-related elements (i.e. Cr, Mn, Cu, and Zn) accounted for 27.5% of PBM variability at NVC. These metals are predominantly released from brake and tire wear, engine oil leakage, and road dust re-suspension. 18,62,95 At the CG site, Zn was the only elemental contributor to PBM variability (21.3%), suggesting that localized emissions from traffic-related sources remain relevant even in suburban settings. This is consistent with previous findings indicating that Zn can persist regionally due to its semi-volatile behavior and association with fine-mode aerosols.96,97

> In general, the distribution of PBM drivers across the two sites reflects fundamental environmental contrasts. While the urban NVC site is characterized by intensive anthropogenic emissions from multiple sectors, the suburban CG site is primarily governed by meteorological processes, with localized Zn emissions playing a secondary role. These insights support the development of sitespecific air quality control strategies: urban areas should prioritize emission mitigation (especially from traffic and fuel combustion), whereas regional management must consider atmospheric mixing and temperature-driven re-emission processes.

du£76 4. Conclusion

This study presents the first year-long dataset of PBM at urban and suburban sites in HCMC, providing novel insights into PBM dynamics in a tropical SEA megacity. Distinct spatial and temporal variations were observed, with higher mean PBM concentrations at the urban site (59.81 ± 29.15 pg m⁻³) compared to the suburban site (26.4 ± 9.59 pg m⁻³). Seasonal trends revealed elevated levels during

684

685

686

687

688

689

ਰੋਂ92

€93

₿94

696

697

699

700

706

707

708

709

710

711

712

713

Downloaded

® **₽**98

Access Article. Published on

Journal Name ARTICLE

the dry season. By applying GAM, this study successfully quantified 14 the nonlinear influences of chemical and meteorological parameters on PBM. The GAM explained 87.7% of PBM variance at 15 the urban site, compared to 41.6% at the suburban site, indicating 716its greater predictive power in emission-rich environments. At the 717 urban site, anthropogenic emissions dominated PBM variability. with industrial and combustion-related elements such as As, Cd, Pb, 719 V, K, Se, and Sb contributing 41%. In contrast, PBM at the suburban $^{720}\,$ site was primarily modulated by temperature (60.8%), Zn (21.3%), and planetary boundary layer height (17.9%), reflecting the stronger role of atmospheric processes in low-emission areas. The finding 22 implied the efficacy of GAM in unraveling complex PBMenvironment interactions, offering a robust framework for source apportionment. Importantly, the observed site-specific drivers suggest that urban areas should prioritize emission controls. targeting traffic and industrial sectors, while suburban management strategies should consider meteorological influences and region \overline{a}^{26} transport mechanisms. Overall, this work provides critical evidence 727 for tailoring Hg mitigation policies to local environmental contexts 728 and emphasizes the utility of flexible, data-driven modeling approaches in advancing atmospheric Hg research and air quality 29 management. On the other hand, we acknowledge certain analytical limitations specific to the current study. Upcoming $^{730}\,$ studies should incorporate expanded datasets that integrate higher time-resolution measurements, detailed chemical speciation of PM,33 and more complete meteorological parameters, together with 734 advanced analytical approaches such as integrated PMF-GAM 736 modeling. 98,99 Such developments will enable a more robu \$\frac{37}{2}\$ identification of source contributions, thereby improving the $\ensuremath{^{738}}$ 739 mechanistic understanding of PBM dynamics in complex $\frac{1}{2}$ 741 atmospheric environments. 742

Author contributions

View Article Online DOI: 10.1039/D5EA00094G

Ly Sy Phu Nguyen: Conceptualization, Methodology, Resources, Supervision, Writing-original draft. Duc Thanh Nguyen: Methodology, Investigation, Data curation, Writing-original draft.

Le Quoc Hau: Investigation, Visualization, Writing-review and editing. Guey-Rong Sheu: Resources, Investigation, Writing-review and editing. To Thi Hien: Conceptualization, Investigation.

Conflicts of interest

The authors declare no conflicts.

Data availability

The data supporting the findings of this study are available from the corresponding author upon reasonable request.

Acknowledgements

This research is funded by University of Science, VNU-HCM under grant number T2024-121.

References

- UNEP, Global Mercury Assessment 2013: Sources, Emissions, Releases and Environmental Transport, Chemicals Branch, Geneva, Switzerland, 2013.
- UN Environment, Global Mercury Assessment 2018, Chemicals and Health Branch, Geneva, Switzerland, 2019.
- L. S. P. Nguyen, L. Zhang, D. W. Lin, N. H. Lin and G. R. Sheu, Eight-year dry deposition of atmospheric mercury to a tropical high mountain background site downwind of the East Asian continent, Environmental Pollution, 2019, 255, 113128, DOI: 10.1016/j.compol.2010.112128

10.1016/j.envpol.2019.113128

 D. Obrist, J. L. Kirk, L. Zhang, E. M. Sunderland, M. Jiskra and N.
 E. Selin, A review of global environmental mercury processes in response to human and natural perturbations: changes of

743 emissions, climate, and land use, Ambio, 2018, 47, 116-147,84 13. Q. Wu, S. Wang, G. Li, S. Liang, C. J. Lin, Y. Wang, and J. Hao, 744 785 DOI: 10.1007/s13280-017-1004-9

- **745** 5. G. R. Sheu, L. S. P. Nguyen, M. T. Truong and D. W. Lin, 86 746 Characteristics of atmospheric mercury at a suburban site i7/87 747 northern Taiwan and influence of trans-boundary haze event 7,88 748 Atmospheric Environment, 2019, 214, 116827, DO7:89 749 10.1016/j.atmosenv.2019.116827 790
 - L. Zhang, S. Wang, L. Wang, Y. Wu, L. Duan, Q. Wu, and X. Li7,91 Updated emission inventories for speciated atmospher 7292 mercury from anthropogenic sources in China, Environment **7**193 Science & Technology, 2015, 49(5), 3185-3194, DO**7**:94 795 10.1021/es504840m

750

751

≱52

₹53

₹54

255

₹56

.₹57

₹58

₹59

₹61

263

₹64

.≇65

₹66

267

768

19

łО

1

773

774

Downloaded on 08/11/25 02:28:01

2025. 762

Open Access Article. Published on 30

- J. Guo, K. Ram, L. Tripathee, S. Kang, J. Huang, P. Chen and 7.96 S. Ghimire, Study on mercury in PM10 at an urban site in th 297 Central Indo-Gangetic plain: seasonal variability an 298 influencing factors, Aerosol and Air Quality Research, 2027,99 20(12), 2729-2740, DOI: 10.4209/aagr.2019.12.0630 800
- **7**60 8. L. S. P. Nguyen, H. Y. Huang, T. L. Lei, T. T. Bui, S. H. Wang, K. **&01** Chi, and N. H. Lin, Characterizing a landmark biomass-burning 02 event and its implication for aging processes during long-range03 transport, Atmospheric Environment, 2020, 241, 117766, DO&O4 10.1016/j.atmosenv.2020.117766
 - L. S. P. Nguyen, G. R. Sheu, T. C. Hsiao, C. T. Lee, S. C. Chang an 806 N. H. Lin, Relationships between atmospheric mercury an 207 optical properties of spring outflow aerosols from Southea 208 Asia, Atmospheric Pollution Research, 2021, 12(10), 101178,09 810 DOI: 10.1016/j.apr.2021.101178
 - 10. P. A. Ariya, M. Amyot, A. Dastoor, D. Deeds, A. Feinberg, G. Ko 3,11 and K. Toyota, Mercury physicochemical and biogeochemical 2 transformation in the atmosphere and at atmospher&13 interfaces: A review and future directions, Chemical Review § 14 19. 2015, 115, 3760-3802, DOI: 10.1021/cr500667e 815
- 775 11. S. M. Dunham-Cheatham, S. Lyman and M. S. Gusti 8,16 776 Comparison and calibration of methods for ambient reactive 17 777 mercury quantification, Science of the Total Environmen8,18 778 2023, 856, 159219, DOI: 10.1016/j.scitotenv.2022.159219 819
- 779 12. L. S. P. Nguyen, G. R. Sheu, S. C. Chang and N. H. Lin, Effects &20 780 temperature and relative humidity on the partitioning &21 781 atmospheric oxidized mercury at a high-altitude mounta 822 background site in Taiwan, Atmospheric Environment, 202823
- 782 783 261, 118572, DOI: 10.1016/j.atmosenv.2021.118572

- Temporal trend and spatial distribution of speciated atmospheric mercury emissions in China during 1978-2014, Environmental Science & Technology, 2016, 50(24), 13428-13435, DOI: 10.1021/acs.est.6b04308
- L. S. P. Nguyen, D. W. Lin, N. H. Lin and G. R. Sheu, Temporal changes in atmospheric mercury concentrations at a background mountain site downwind of the East Asia continent in 2006-2016, Science of the Total Environment, 2019, 686, 1049-1056, DOI: 10.1016/j.scitotenv.2019.05.425
- X. Fu, H. Zhang, X. Feng, Q. Tan, L. Ming, C. Liu and L. Zhang, Domestic and transboundary sources of atmospheric particulate bound mercury in remote areas of China: evidence from mercury isotopes, Environmental Science & Technology, 2019, 53(4), 1947-1957, DOI: 10.1021/acs.est.8b06736
- D. Han, J. Zhang, Z. Hu, Y. Ma, Y. Duan, Y. Han, and W. Wang, Particulate mercury in ambient air in Shanghai, China: sizespecific distribution, gas-particle partitioning, and association with carbonaceous composition, Environmental Pollution, 2018, 238, 543-553, DOI: 10.1016/j.envpol.2018.03.088
- K. Marumoto, N. Suzuki, Y. Shibata, A. Takeuchi, A. Takami, N. Fukuzaki, and M. Saito, Long-term observation of atmospheric speciated mercury during 2007-2018 at Cape Hedo, Okinawa, Japan. Atmosphere, 2019, 10(7), 362, DOI: 10.3390/atmos10070362
- L. S. P. Nguyen, T. T. Hien, M. T. Truong, N. D. T. Chi and G. R. Sheu, Atmospheric particulate-bound mercury (PBM₁₀) in a Southeast Asia megacity: sources and health risk assessment, Chemosphere. 2022. 307. 135707. DOI: 10.1016/j.chemosphere.2022.135707
- J. Guo, C. M. Sharma, L. Tripathee, S. Kang, X. Fu, J. Huang, and P. Chen, Source identification of atmospheric particle-bound mercury in the Himalayan foothills through non-isotopic and isotope analyses, Environmental Pollution, 2021, 286, 117317, DOI: 10.1016/j.envpol.2021.117317
- K. Li, D. J. Jacob, H. Liao, L. Shen, Q. Zhang and K. H. Bates, Anthropogenic drivers of 2013-2017 trends in summer surface ozone in China, Proceedings of the National Academy of Sciences, 2019, 422-427, DOI: 116(2), 10.1073/pnas.1812168116
- 824 21. X. Xu, Y. Liao, I. Cheng and L. Zhang, Potential sources and processes affecting speciated atmospheric mercury at

834

§35

₹36

₹37

ਨੂੰ38

₹39

. \$40

841

842

843

É44

248

849

\$50

851

12

3

35

856

857

858

859

on 08/11/25 02:28:01

Downloaded

2025. 845

30 **8**46

Published on 847

Open Access Article.

Journal Name ARTICLE

826 Kejimkujik National Park, Canada: comparison of recept 268 827 models and data treatment methods, Atmospheric Chemist & 69 828 and Physics, 2017, 17(2), 1381-1400, DOI: 10.5194/acp-1870 31. N. D. Dat, L. S. P. Nguyen, T. D. H. Vo, T. Van Nguyen, T. T. L. 829 871 1381-2017

- 830 22. Y. H. Taguchi, Unsupervised Feature Extraction Applied \$\frac{16}{2}\$ 831 Bioinformatics: A PCA Based and TD Based Approach, Spring 273 832 Nature, 2024, DOI: 10.1007/978-3-031-60982-4
 - 23. M. T. Truong, L. S. P. Nguyen, T. T. Hien, T. D. H. Pham and T. **8.75** L. Do, Source apportionment and risk estimation of hea\\$76 metals in PM₁₀ at a Southern Vietnam megacity, Aerosol an 877 2022. 220094. D0878 Quality Research, 22(8). 879 10.4209/aagr.220094
 - 24. B. Xu, H. Xu, H. Zhao, J. Gao, D. Liang, Y. Li, and G. Shi, Sour 80 apportionment of fine particulate matter at a megacity 881 China, using an improved regularization supervised PM\$82 model, Science of the Total Environment, 2023, 879, 163198,83 DOI: 10.1016/j.scitotenv.2023.163198 884
 - 25. K. Ravindra, P. Rattan, S. Mor and A. N. Aggarwal, Generalize 85 additive models: building evidence of air pollution, clima 886 change and human health, Environment International, 201887 132, 104987, DOI: 10.1016/j.envint.2019.104987
 - 26. S. N. Wood, Stable and efficient multiple smoothing paramet 889 estimation for generalized additive models, Journal of th 290 American Statistical Association, 2004, 99(467), 673-686, DO&91 10.1198/016214504000000980
 - 27. Q. Wu, Y. Tang, S. Wang, L. Li, K. Deng, G. Tang, and H. Zhan §93 Developing a statistical model to explain the observed declin&94 of atmospheric mercury, Atmospheric Environment, 2028,95 243, 117868, DOI: 10.1016/j.atmosenv.2020.117868
 - 28. Q. Wu, Y. Tang, L. Wang, S. Wang, D. Han, D. Ouyang, and J. H&97 Impact of emission reductions and meteorology changes 6898 atmospheric mercury concentrations during the COVID-1899 lockdown, Science of the Total Environment, 2021, 759,00 142323, DOI: 10.1016/j.scitotenv.2020.142323 901
- 860 29. J. D. Krug, A. Dart, C. L. Witherspoon, J. Gilberry, Q. Malloy, 9.02 861 Kaushik and R. W. Vanderpool, Revisiting the size selective03 862 performance of EPA's high-volume total suspended particula \$\omega 04\$ 863 matter (Hi-Vol TSP) sampler, Aerosol Science and Technolog 9,05 864 2017, 51(7), 868-878, DOI: 10.1080/02786826.2017.131635\(\&\text{906} \)
- 865 30. T. T. Hien, N. D. T. Chi, N. T. Nguyen, L. X. Vinh, N. Takenaka an 907 866 D. H. Huy, Current status of fine particulate matter (PM_{2.5}) 608 38. H. Y. Huang, S. H. Wang, W. X. Huang, N. H. Lin, M. T. Chuang, 867 Vietnam's most populous city, Ho Chi Minh City, Aerosol an 909

- Air Quality Research, 2019, 19(10), 2239-2251 DOI: DOI: 10.1039/D5EA00094G 10.4209/aaqr.2018.12.0471
- Do, A. T. K. Tran and N. T. T. Hoang, Pollution characteristics, associated risks, and possible sources of heavy metals in road dust collected from different areas of a metropolis in Vietnam, Environmental Geochemistry and Health, 2023, 45(11), 7889-7907, DOI: 10.1007/s10653-023-01696-4
- T. T. Hien, L. S. P. Nguyen, M. T. Truong, T. D. H. Pham, T. A. Ngan, T. H. Minh, and N. T. Nguyen, Spatiotemporal variations of atmospheric mercury at urban and suburban areas in Southern Vietnam megacity: A preliminary year-round measurement study, Atmospheric Environment, 2024, 333, 120664, DOI: 10.1016/j.atmosenv.2024.120664
- L. S. P. Nguyen, T. D. H. Pham, M. T. Truong and A. N. Tran, Characteristics of total gaseous mercury at a tropical megacity in Vietnam and influence of tropical cyclones, Atmospheric Pollution 2023, 14(8), DOI: Research. 101813. 10.1016/j.apr.2023.101813
- D. S. McLagan, F. Monaci, H. Huang, Y. D. Lei, C. P. Mitchell and F. Wania, Characterization and quantification of atmospheric mercury sources using passive air samplers, Journal of Geophysical Research: Atmospheres, 2019, 124(4), 2351-2362, DOI: 10.1029/2018JD029373
- 892 35. J. Zheng, M. Li, B. Tang, W. Luo, Y. Ma, M. Ren, and B. Mai, Levels, spatial distribution, and impact factors of heavy metals in the hair of metropolitan residents in China and human health implications, Environmental Science & Technology, 2021, 55(15), 10578-10588, DOI: 10.1021/acs.est.1c02001
 - N. D. Dat, M. T. Truong, L. S. P. Nguyen, A. T. K. Tran, N. M. Duc, T. D. H. Vo and G. R. Sheu, Street dust mercury levels among different land-use categories in Ho Chi Minh City, Vietnam: Source apportionment and risk estimation, Atmospheric DOI: Pollution Research. 2023. 14(1), 101623. 10.1016/j.apr.2022.101623
 - R. Gelaro, W. McCarty, M. J. Suárez, R. Todling, A. Molod, L. Takacs, and B. Zhao, The modern-era retrospective analysis for research and applications, version 2 (MERRA-2), Journal of Climate, 2017, 30(14), 5419-5454, DOI: 10.1175/JCLI-D-16-0758.1
 - A. M. da Silva and C. M. Peng, Influence of synoptic-dynamic

910		meteorology	on the lo	ong-range	trans	port of Indochi	na bioı	ma £ 52
911		burning ae	rosols,	Journal	of	Geophysical	Resea	arc 19 .53
912		Atmospheres	s, 202	.0, 125	(3),	e2019JD0312	60,	DO9:54
913		10.1029/2019	9JD0312	.60				955
914	39.	V. Buchard. (C. A. Rar	ndles. A. I	И. Da	Silva, A. Darm	enov.	р. 9 .56

- 39. V. Buchard, C. A. Randles, A. M. Da Silva, A. Darmenov, P. 8.56 915 Colarco, R. Govindaraju, and H. Yu, The MERRA-2 aeros 9157 916 reanalysis, 1980 onward. Part II: Evaluation and case studie 9,58 917 Journal of Climate, 2017, 30(17), 6851-6872, DO9:59 918 960 doi.org/10.1175/JCLI-D-16-0613.1
- **9**19 40. R. R. Draxler and G. D. Rolph, HYSPLIT (Hybrid single-partic \$\overline{9}61\$ 52. <u>9</u>20 lagrangian integrated trajectory) model access via NOAA AR 1262 ₹21 READY, NOAA Air Resources Laboratory, Silver Spring, M9,63 922 2013, DOI: http://www.arl.noaa.gov/HYSPLIT.php
 - 41. S. H. Wang, W. T. Hung, S. C. Chang and M. C. Yen, Transpoæ65 characteristics of Chinese haze over Northern Taiwan 966 winter, 2005-2014, Atmospheric Environment, 2016, 126, 76967 86, DOI: 10.1016/j.atmosenv.2015.11.043 968

Downloaded on 08/11/25 02:28:01

2025. 929

30 ₹30

Published on

<u>9</u>23

<u> \$</u>24

₫25

926

927

£28

<u>9</u>32

933

934

935

6

8

3

- pollution, traffic volume and meteorology, Atmospher 270 Environment, 2005. 39. 2145-2155, DO9:71 972 10.1016/i.atmosenv.2004.12.020
- **9**31 43. S. N. Wood, Generalized Additive Models: An Introduction with 973 R, Chapman & Hall/CRC, 2017, DOI: 10.1201/978131537027974
 - 44. T. Hastie, R. Tibshirani, J. H. Friedman and J. H. Friedman, Th. 75 elements of statistical learning: data mining, inference, an 976 prediction, Vol. 2, 1-758, Springer, New York, 2009. 977
 - 45. T. J. Hastie, Generalized additive models, Statistical Models 978 S, 2017, 249-307. 979
 - 46. T. Fushiki, Estimation of prediction error by using K-fold cros 980 validation, Statistics and Computing, 2011, 21, 137-146, DOB81 10.1007/s11222-009-9153-8 982
- 941 47. Y. Jung, Multiple predicting K-fold cross-validation for mod **983** 942 selection, Journal of Nonparametric Statistics, 2018, 30(19,84 943 197-215, DOI: 10.1080/10485252.2017.1404598 985
- 944 48. L. A. Yates, Z. Aandahl, S. A. Richards and B. W. Brook, Cros886 945 validation for model selection: a review with examples fro 87
- 946 ecology, Ecological Monographs, 2023, 93(1), e1557, DO9:88 947 10.1002/ecm.1557 989
- 948 49. G. Xiu, J. Cai, W. Zhang, D. Zhang, A. Büeler, S. Lee, and 9.90 949 Zhang, Speciated mercury in size-fractionated particles 991
- 950 Shanghai ambient air, Atmospheric Environment, 2009, 43(19),92 59. 951 993 3145-3154, DOI: 10.1016/j.atmosenv.2008.07.044

- 50. X. Qin, X. Dong, C. Liu, R. Wei, Z. Tao, H. Zhang and Q. Guo, Mass-independent fractionation of mercury stable isotopes reveals atmospheric transport impact on particulate-bound mercury, Geophysical Research Letters, 2025, 52(17), e2025GL116080, DOI: 10.1029/2025GL116080
 - B. Liu, G. J. Keeler, J. T. Dvonch, J. A. Barres, M. M. Lynam, F. J. Marsik and J. T. Morgan, Temporal variability of mercury speciation in urban air, Atmospheric Environment, 2007, 41(9), 1911-1923, DOI: 10.1016/j.atmosenv.2006.10.063
- S. H. Kim, Y. J. Han, T. M. Holsen and S. M. Yi, Characteristics of atmospheric speciated mercury concentrations (TGM, Hg(II) and Hg(p)) in Seoul, Korea, Atmospheric Environment, 2009, 43(20), 3267-3274, DOI: 10.1016/j.atmosenv.2009.02.038
- H. Xu, J. E. Sonke, B. Guinot, X. Fu, R. Sun, A. Lanzanova, and J. Cao, Seasonal and annual variations in atmospheric Hg and Pb isotopes in Xi'an, China, Environmental Science & Technology, 2017, 51(7), 3759-3766, DOI: 10.1021/acs.est.6b06145
- 42. M. Aldrin and I. H. Haff, Generalised additive modelling of a 49.69 54. L. Xu, J. Chen, L. Yang, Z. Niu, L. Tong, L. Yin and Y. Chen, Characteristics and sources of atmospheric mercury speciation in a coastal city, Xiamen, China, Chemosphere, 2015, 119, 530-539, DOI: 10.1016/j.chemosphere.2014.07.024
 - H. Pyta and W. Rogula-Kozłowska, Determination of mercury in size-segregated ambient particulate matter using CVAAS, Microchemical Journal, 2016, 124, 76-81, DOI: 10.1016/j.microc.2015.08.001
 - X. Ren, W. T. Luke, P. Kelley, M. D. Cohen, R. Artz, M. L. Olson, and J. W. Stehr, Atmospheric mercury measurements at a suburban site in the Mid-Atlantic United States: inter-annual, seasonal and diurnal variations and source-receptor relationships, Atmospheric Environment, 2016, 146, 141-152, DOI: 10.1016/j.atmosenv.2016.08.028
 - L. Poissant, M. Pilote, C. Beauvais, P. Constant and H. H. Zhang, A year of continuous measurements of three atmospheric mercury species (GEM, RGM and Hgp) in southern Quebec, Canada, Atmospheric Environment, 2005, 39(7), 1275-1287, DOI: 10.1016/j.atmosenv.2004.11.007
 - D. M. Feddersen, R. Talbot, H. Mao and B. C. Sive, Size distribution of atmospheric particulate mercury in marine and coastal atmospheres, Atmospheric Chemistry & Physics Discussions, 2012, 12(6), DOI: 10.5194/acpd-12-14591-2012
 - X. Li, L. Liu, Y. Wang, G. Luo, X. Chen, X. Yang, and X. He, Heavy metal contamination of urban soil in an old industrial city

103

1004

1**0**05

[©]21<u>₹</u>06

201<u>6</u>07 201<u>6</u>07 21<u>6</u>08

ଅ**1@**10

월1011

∆21€12

Š1**0**13

ਤੂੰ1**ਰ**15

ੂ 1€16 16

ີ⊍1**∯**17

₹1**0**18

\$1019

lЮ

1

2

1024

1025

1027

1028

1029

1031

1032

1033

1034

Journal Name ARTICLE

994 (Shenyang) in Northeast China, Geoderma, 2013, 192, 50-1835 68. B. de Foy, J. Heo, J. Y. Kang, H. Kim and J. J. Schauer, Source 995 DOI: 10.1016/j.geoderma.2012.08.011 1036 996 60. T. B. Councell, K. U. Duckenfield, E. R. Landa and E. Callend 20,37

- 997 Tire-wear particles as a source of zinc to the environme. 1838 998 Environmental Science & Technology, 2004, 38(15), 4206939 999 4214, DOI: 10.1021/es034631f
- 1000 61. M. Keane, A. Siert, S. Stone and B. T. Chen, Profiling stainl \$\alpha 41\$ steel welding processes to reduce fume emissions, hexaval <u>40</u>42 1002 chromium emissions and operating costs in the workplate43 Journal of Occupational and Environmental Hygiene, 2016,44 13(1), 1-8, DOI: 10.1080/15459624.2015.1072634
 - 62. J. Sternbeck, Å. Sjödin and K. Andréasson, Metal emissid 646 from road traffic and the influence of resuspension-result 647 from two tunnel studies, Atmospheric Environment, 2010,48 36(30), 4735-4744, DOI: 10.1016/S1352-2310(02)00561-7 1049
 - 63. Z. Bozkurt, O. E. Gaga, F. Taşpınar, A. Arı, B. Pekey, H. Pek 🗜 0,50 71. S. Illuminati, A. Annibaldi, S. Bau, C. Scarchilli, V. Ciardini, P. and Ö. Özden Üzmez, Atmospheric ambient trace elem4051 concentrations of PM₁₀ at urban and sub-urban sites: sou**1**@52 apportionment and health risk estimation, Environment 9153 Monitoring and Assessment, 2018, 190, 1-17, D100:54 10.1007/s10661-018-6517-6 1055 72.
 - 64. L. S. P. Nguyen, T. T. L. Do, T. G. H. Vo, Q. H. Le and T. T. Hi**a**0,56 The source and distribution of heavy metals in the atmosph 4.657 across Southeast Asia, in Heavy Metal Remediati**a**.**0**.58 Sustainable Nexus Approach, Springer Nature Switzerla 10,59 Cham, 2024, 1–26, DOI: 10.1007/978-3-031-53688-5_1
 - 65. B. Chen, A. F. Stein, P. G. Maldonado, A. M. S. de la Campa 1061 73. Gonzalez-Castanedo, N. Castell and J. D. de la Rosa, \$\,\overline{12}\,\overline{62}\$ distribution and concentrations of heavy metals 1063 atmospheric aerosols originating from industrial emissions 1264 predicted by the HYSPLIT model, Atmospheric Environme 10,65 2013, 71, 234–244, DOI: 10.1016/j.atmosenv.2013.02.013 1066
- 1026 66. Y. Dai, H. Dong, L. Sun, J. Li, T. Zhang, Y. Geng and Z. Liu, 110267 cycle environmental impact assessment of titanium diox 10268 Review, 2024, 105, 107412, DOI: 10.1016/j.eiar.2023.107412070
- 1030 67. M. Keane, S. Stone, B. Chen, J. Slaven, D. Schwegler-Berry and 71 J. Antonini, Hexavalent chromium content in stainless st 2072 welding fumes is dependent on the welding process and shi**2**073 gas type, Journal of Environmental Monitoring, 2009, 11(20),74 1075 418-424, DOI: 10.1039/B814063D

- attribution of air pollution using a generalized additive model and particle trajectory clusters, Science of the Total DOI: Environment, 2021. 780. 146458. 10.1016/j.scitotenv.2021.146458
- X. Fu, M. Jiskra, X. Yang, N. Marusczak, M. Enrico, J. Chmeleff, and J. E. Sonke, Mass-independent fractionation of even and odd mercury isotopes during atmospheric mercury redox reactions, Environmental Science & Technology, 2021, 55(14), 10164-10174, DOI: 10.1021/acs.est.1c02568
- 70. L. S. P. Nguyen and T. T. Hien, Long-range atmospheric mercury transport from across East Asia to a suburban coastal area in Southern Vietnam, Bulletin of Environmental Contamination and Toxicology, 2024, 112(1), 14, DOI: 10.1007/s00128-023-03842-1
- Grigioni, and C. Truzzi, Seasonal evolution of size-segregated particulate mercury in the atmospheric aerosol over Terra Nova Bay, Antarctica, Molecules, 2020, 25(17), 3971, DOI: 10.3390/molecules25173971
- H. Zhou, C. Zhou, P. K. Hopke and T. M. Holsen, Mercury wet deposition and speciated mercury air concentrations at rural and urban sites across New York State: temporal patterns, sources and scavenging coefficients, Science of the Total Environment, 2018, 637. 943-953, DOI: 10.1016/j.scitotenv.2018.05.047
- Y. J. Han, J. E. Kim, P. R. Kim, W. J. Kim, S. M. Yi, Y. S. Seo and S. H. Kim, General trends of atmospheric mercury concentrations in urban and rural areas in Korea and characteristics of highconcentration events, Atmospheric Environment, 2014, 94, 754-764, DOI: 10.1016/j.atmosenv.2014.06.002
- G. L. Simpson, Modelling palaeoecological time series using generalised additive models, Frontiers in Ecology and Evolution, 2018, 6, 149, DOI: 10.3389/fevo.2018.00149
- production in China, Environmental Impact Assessma 069 75. D. N. Asimakopoulos, T. Maggos and C. Vasilakos, Particulate matter levels in a suburban Mediterranean area: Analysis of a 53-month long experimental campaign, Journal of Hazardous Materials, 2010, 182. 801-811, DOI: 10.1016/j.jhazmat.2010.06.108
 - 76. C. Y. Hsu, K. H. Chi, C. D. Wu, S. L. Lin, W. C. Hsu, C. C. Tseng, and Y. C. Chen, Integrated analysis of source-specific risks for PM_{2.5}-bound metals in urban, suburban, rural, and industrial

1077	areas, Environmental Pollution, 2021, 275, 116652, D D1:1
1078	10.1016/j.envpol.2021.116652 111
1079	7 P Bertaccini V Dukic and R Ignaccolo Modeling the sh drfl-2

- 1080 term effect of traffic and meteorology on air pollution in Tulib21 1081 with generalized additive models, Advances in Meteorolo 1,122 1082 2012, 2012, 609328, DOI: 10.1155/2012/609328
- 1083 78. L. Yang, G. Qin, N. Zhao, C. Wang and G. Song, Using 124 1084 generalized additive model with autoregressive terms to stuld/25 1085 the effects of daily temperature on mortality, BMC Medital26 1086 Research Methodology, 2012, 12(1), 165, DOI: 10.1186/1411-27 2288-12-165

1087

1688

2 2 1 2 89

Ë1̈́890

ଅ**1@**93

음1**0**94

å1**€**95

§1**0**96

[≈]1**७**97

g1**0**98

Publish 1699

ື 1<u></u>300

∄1<u>‡</u>01

§1102

1107

1108

1109

- 79. A. F. Zuur, E. N. Ieno and G. M. Smith, Analysing Ecologital 29 Data, Springer, New York, 2007, DOI: 10.1007/978-0-3**11**-30 45972-1 12
- 21. 1991 80. C. T. Driscoll, R. P. Mason, H. M. Chan, D. J. Jacob and 11.32 Pirrone, Mercury as a global pollutant: sources, pathways, ahl 33 effects, Environmental Science & Technology, 2013, 47(101,34) 4967-4983, DOI: 10.1021/es305071v
 - 81. N. Pirrone, S. Cinnirella, X. Feng, R. B. Finkelman, H. R. Frie 11,36 J. Leaner, and K. Telmer, Global mercury emissions to the 37 atmosphere from anthropogenic and natural source 138 Atmospheric Chemistry and Physics, 2010, 10(13), 5951-5964,39 DOI: 10.5194/acp-10-5951-2010 1140
 - 82. U. Kurien, Z. Hu, H. Lee, A. P. Dastoor and P. A. Ariya, Radiat **b 1** enhanced uptake of Hg⁰(g) on iron (oxyhydr)oxible42 nanoparticles, RSC Advances, 2017, 7(71), 45010-45021, D101:43 10.1039/C7RA07401H
 - 83. E. Gaggero, M. J. López-Muñoz, M. C. Paganini, A. Arencibia 145 Bertinetti, N. Fernández de Paz and P. Calza, Mercury ahld46 organic pollutants removal from aqueous solutions 161/47 heterogeneous photocatalysis with ZnO-based material 1,48 Molecules, 2023, 28(6), 2650, D**1**01:49 10.3390/molecules28062650 1150
- 1110 84. F. Yue, H. Angot, H. Liu and Z. Xie, Marine phytoplankton ah 1051 1111 sea-ice initiated convection drive spatiotemporal differendes52 1112 Arctic summertime mercury rebound. Natúlr2e53 1113 Communications, 2025, 16(1), 6075, DOI: 10.1038/s4146154 1114 025-61000-z
- 1115 85. Z. Xu, L. Chen, Y. Zhang, G. Han, Q. Chen, Z. Chu, and X. Wall 56 1116 Meteorological drivers of atmospheric mercury seasonality 1657 1117 the temperate Northern Hemisphere, Geophysical Resealch58

- e2022GL100120 Article Online Letters, 2022, 49(20), DOI: 10.1039/D5EA00094G 10.1029/2022GL100120
- 86. A. M. S. de la Campa, J. D. de la Rosa, J. C. Fernández-Caliani and Y. González-Castanedo, Impact of abandoned mine waste on atmospheric respirable particulate matter in the historic mining district of Rio Tinto (Iberian Pyrite Belt), Environmental Research, 2011, 111(8), 1018-1023, 10.1016/j.envres.2011.07.001
- S. Jain, S. K. Sharma, T. K. Mandal and M. Saxena, Source apportionment of PM₁₀ in Delhi, India using PCA/APCS, UNMIX and PMF, Particuology, 2018, 37, 107-118, 10.1016/j.partic.2017.05.009
- W. Li, P. Ge, M. Chen, J. Tang, M. Cao, Y. Cui, and D. Nie, Tracers from biomass burning emissions and identification of biomass burning. Atmosphere, 2021, 12(11), 10.3390/atmos12111401
- H. Wen and J. Carignan, Reviews on atmospheric selenium: emissions, speciation and fate, Atmospheric Environment, 2007. DOI: 41(34), 7151-7165. 10.1016/j.atmosenv.2007.07.035
- K. Guo, Y. Li, J. Wang, Z. Sui, T. Wang and W. P. Pan, A review on selenium in coal-fired power plants: content and forms in coal, determination methods, migration, transformation, and control technologies, Journal of Environmental Chemical Engineering, 2024, 12(5), 113579, DOI: 10.1016/j.jece.2024.113579
- 1144 91. S. Ma, F. Xu, D. Qiu, S. Fan, R. Wang, Y. Li and X. Chen, The occurrence, transformation and control of selenium in coalfired power plants: status quo and development, Journal of the Air & Waste Management Association, 2022, 72(2), 131-146, DOI: 10.1080/10962247.2021.2010620
 - J. Yu, C. Yan, Y. Liu, X. Li, T. Zhou and M. Zheng, Potassium: a tracer for biomass burning in Beijing?, Aerosol and Air Quality 2447-2459, DOI: Research, 2018. 18(9), 10.4209/aaqr.2017.11.0536
 - V. I. Babushok, P. Deglmann, R. Krämer and G. T. Linteris, Influence of antimony-halogen additives on propagation, Combustion Science and Technology, 2017, 189, 290-311, DOI: 10.1080/00102202.2016.1208187.
 - J. Das, A. Kleiman, A. U. Rehman, R. Verma and M. H. Young, The cobalt supply chain and environmental life cycle impacts

1165

1166

1167

Journal Name ARTICLE

, Sustainabil 1t)1,7 6	of lithium-ion battery energy storage systems,		1159
1177	2024, 16(5), 1910, DOI: 10.3390/su16051910		1160
s from chro 1 n1e78	. M. J. Pilat and R. C. Pegnam, Particle emission	95.	1161
40(8), 639-6 44,7 9	plating, Aerosol Science and Technology, 2006,		1162
1180	DOI: 10.1080/02786820600763020		1163

- 96. W. H. Liao, S. Takano, H. A. Tian, H. Y. Chen, Y. Sohrin and T1181 Ho, Zn elemental and isotopic features in sinking particles1df82 the South China Sea: Implications for its sources and sink1,83 Geochimica et Cosmochimica Acta, 2021, 314, 68-84, D10184 10.1016/j.gca.2021.09.013
- 97. M. Pirhadi, A. Mousavi, S. Taghvaee, M. M. Shafer and 10.86 Sioutas, Semi-volatile components of PM_{2.5} in an urbland 87 environment: volatility profiles and associated oxidat 10.488 potential, Atmospheric Environment, 2020, 223, 117197, D10.189 10.1016/j.atmosenv.2019.117197 1190
- 98. L. Guan, Y. Liang, Y. Tian, Z. Yang, Y. Sun and Y. Fe14,91 Quantitatively analyzing effects of meteorology and PM $_{2.5}$

- sources on low visual distance, Science of the three Total Environment, 2019, 659, DOI: 10.1039/D5EA00094G DOI: 10.1016/j.scitotenv.2018.12.431
- Quantifying role of source variations on PM_{2.5}-bound toxic components under climate change: measurement at multiple sites during 2018-2022 in a Chinese megacity, Journal of Hazardous Materials, 2025, 138584, DOI: 10.1016/j.jhazmat.2025.138584
- 100. I. Cheng, L. Zhang, P. Blanchard, J. Dalziel and R. Tordon, Concentration-weighted trajectory approach to identifying potential sources of speciated atmospheric mercury at an urban coastal site in Nova Scotia, Canada, Atmospheric Chemistry and Physics, 2013, 13(12), 6031-6048, DOI: 10.5194/acp-13-6031-2013

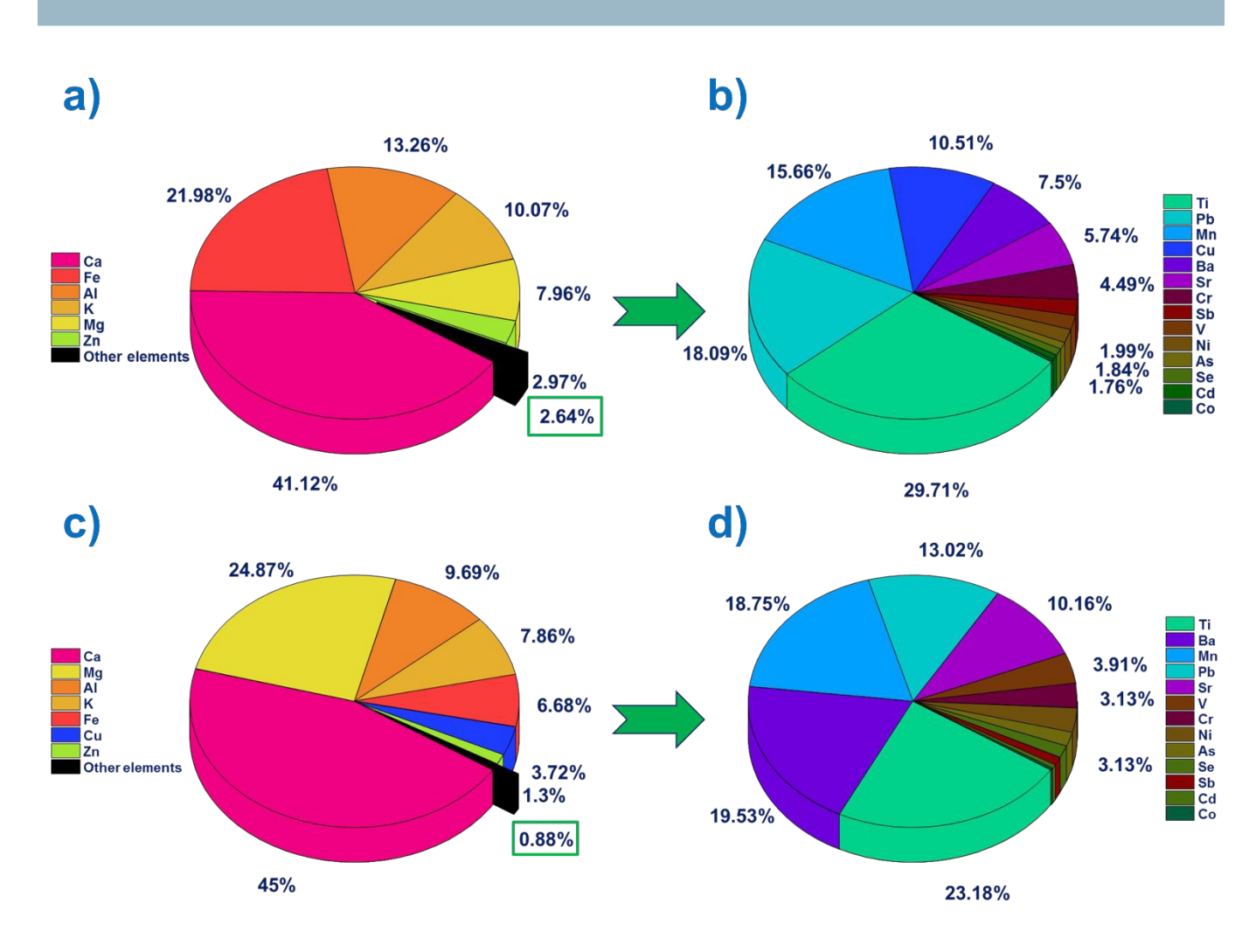


Fig. 1 Pie charts illustrating the percentage (%) of elements TSP samples collected from urban and suburban areas: (a) and (c) show major elements in urban and suburban areas, respectively; (b) and (d) show trace elements in urban and suburban areas, respectively.

Open Access Art<u>Id</u>e. Published on 3th 2025. Downloaded on 08/11/25 02:28:01.

Journal Name ARTICLE

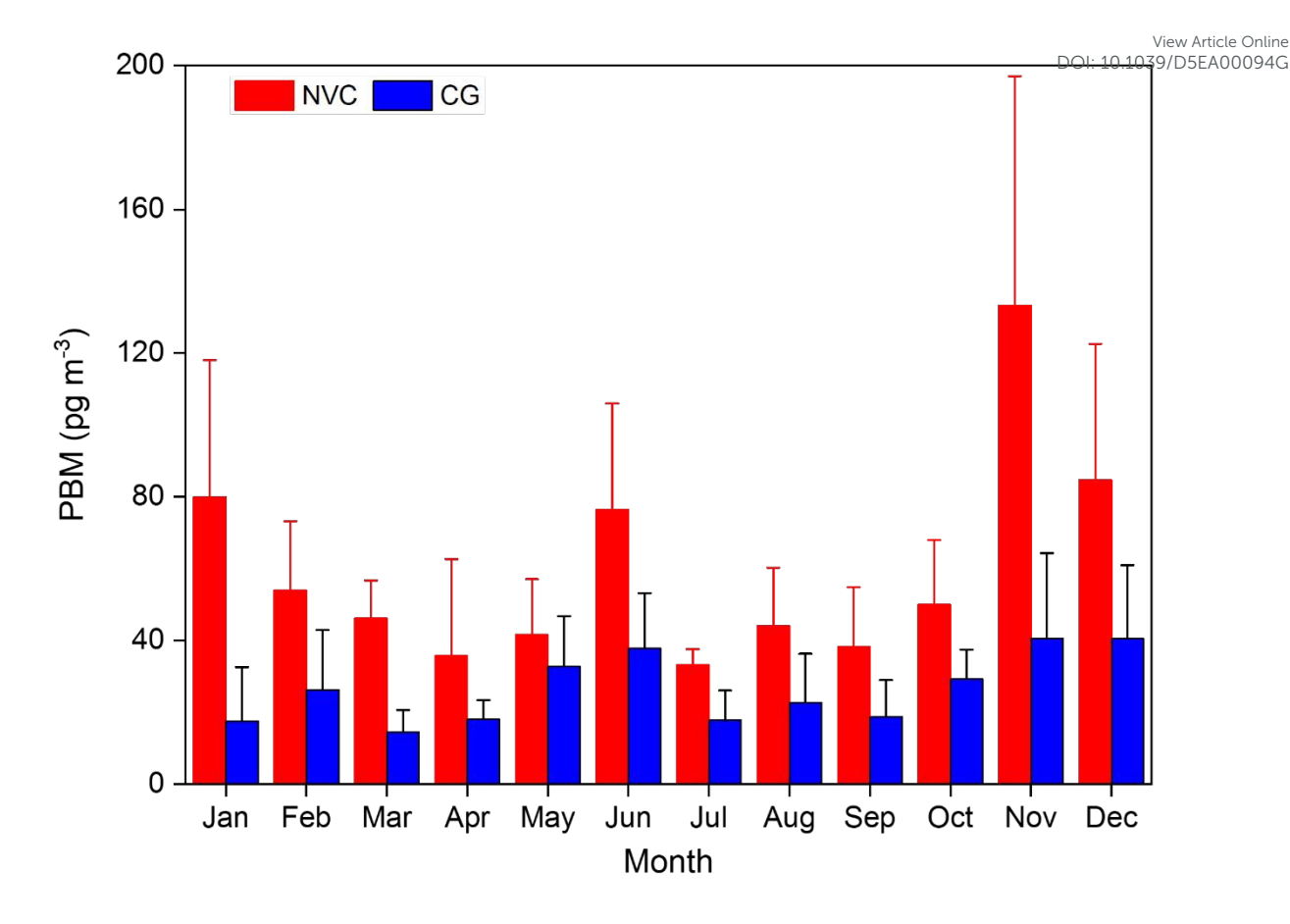


Fig. 2 Monthly variation of PBM concentration (pg m⁻³) at two sites, Nguyen Van Cu and Can Gio, from May 2022 to April 2023

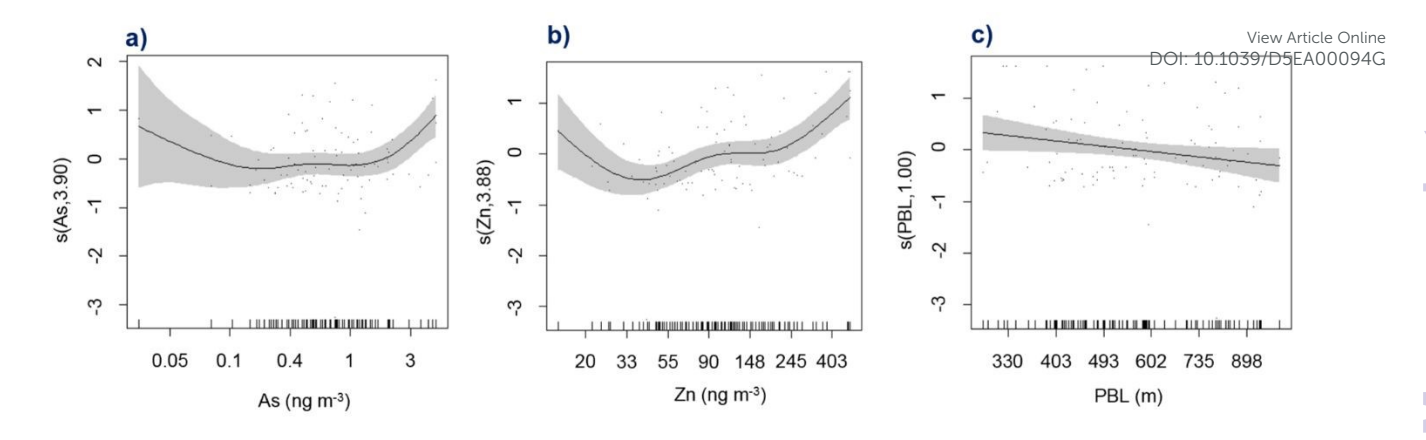


Fig. 3 Spline plots illustrate the relationships between PBM concentration and elemental concentrations at the NVC monitoring site: (a) As, (b) Zn, and (c) PBL - the meteorological parameter. The y-axis represents the spline values of PBM as a function of each independent variable, and the x-axis corresponds to the observed values of each independent variable. The solid line indicates the fitted spline, while the shaded area around it represents the 95% confidence interval for the predicted response. Tick marks on the x-axis show the distribution of the data points. The number in parentheses in each y-axis label denotes the estimated degrees of freedom (EDF). Dots in the plots represent residual values.

119

Open Access Article. Published on 30 72025. Dokyloads on 成11/4202:2201. The This article is licensed under Creatise Company Apriluman 3.名 proded Lice

Open Access Article. Published on 30 2025. Downloaded on 2011/25 位:28:位. 7 This article is licensed under a Creative Commons 包tributio 30:0 包ported 包cence.

Journal Name ARTICLE

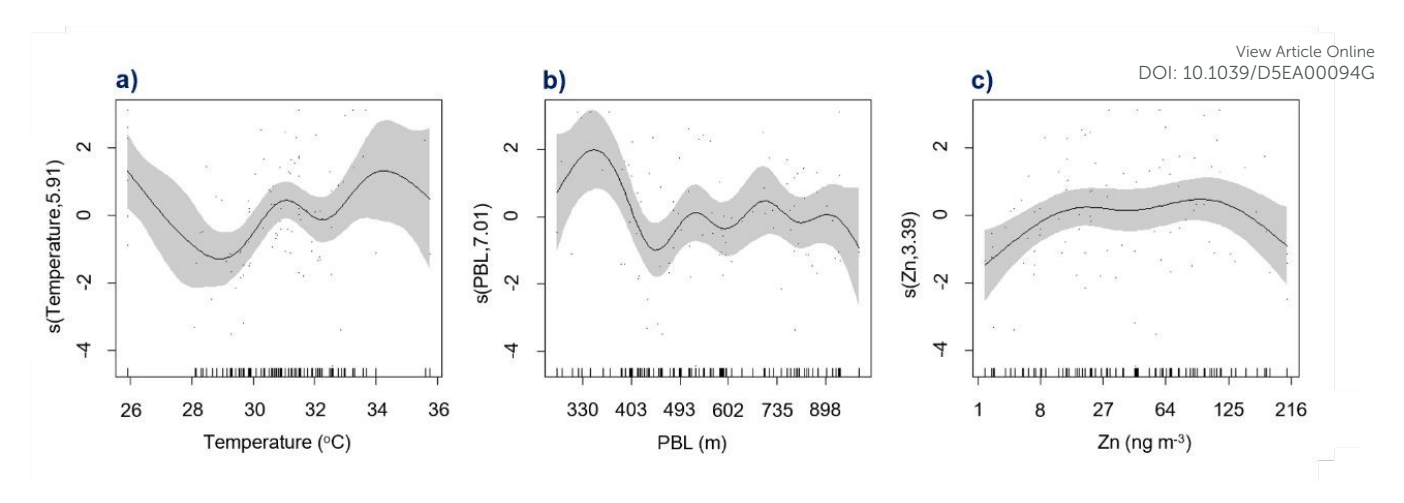


Fig. 4 Spline plots illustrate the relationships between PBM concentration and elemental concentrations at the CG monitoring site: (a)

Temperature, (b) PBL, and elemental concentration: (c) Zn.



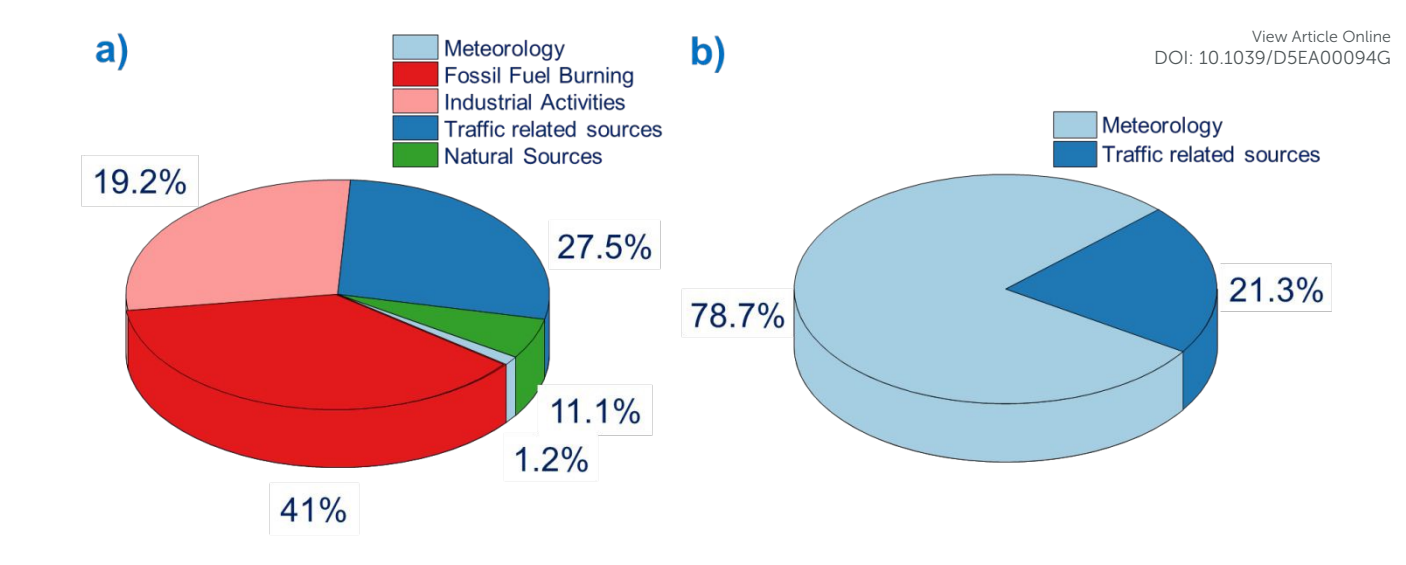


Fig. 5 Source category contributions to PBM variability at the two sampling sites (a) urban and (b) suburban

Journal Name

ARTICLE

Table 1. Comparison of PBM concentrations (pg m⁻³) in samples with values reported in other countries worldwide.

View Article Online DOI: 10.1039/D5EA00094G

Site	Size	Туре	Year	PBM (pg m ⁻³)	References
NVC, Vietnam	TSP	Urban	2022-2023	59.81 ± 29.15	This study
CG, Vietnam	TSP	Suburban	2022-2023	26.4 ± 9.59	This study
Beijing, China	TSP	Urban	2016 - 2017	210.1 ± 146.2	50
Kathmandu Valley, Nepal	TSP	Urban	2013-2014	850.5 ± 926.8	19
Shanghai, China	TSP	Urban	2004-2006	560 ± 220, 330 ± 90	49
Grianginal, Grinia		C 1.24.1	200 : 2000	(2 sites)	
Xi'an, China	TSP	Urban	2010-2013	640 ± 540	53
Detroit, USA	PM _{2.5}	Urban	2006	20.8 ± 30	51
Seoul, Korea	PM _{2.5}	Urban	2005-2006	23.9 ± 19.6	52
Xiamen, China	TSP	Suburban	2012-2013	174.1 ± 160.9	54
Dhulikhel, Nepal	TSP	Suburban	2018	108.7 ± 86.2	19
Okinawa, Japan	PM _{2.5}	Suburban	2009-2018	2.6 ± 3.6	17
Zabrze, Poland	TSP	Suburban	2013	65.5 ± 53.7	55
Zabrze, Poland	PM_{10}	Suburban	2013	63.6 ± 53.0	55
Nova Scotia, Canada	PM _{2.5}	Suburban	2010-2011	2.32 ± 3.09	100
Beltsville, Maryland, USA	PM _{2.5}	Suburban	2007-2015	8.6 ± 56.8	56
High mountain in					
central Taiwan,	$PM_{2.5}$	Suburban	2009-2016	3.1 ± 8.5	3
Taiwan					
aoyuan City, Taiwan	PM _{2.5}	Suburban	2017-2018	18.7 ± 86.8	5

1216

This article is licensed under a Creative Commons Attribution 3.0 Unported Licence.

Dopen Access Article. Published on 30 2025. Downloaded on 08/11/25 02:28:01.

This article is licensed under a Creative Commons Attribution 3.0 Unp

Data availability

The data supporting the findings of this study are available from the corresponding author upon reasonable request.